












12,13-diHOME protects against the age-related decline in cardiovascular function via attenuation of CaMKII

Received: 8 April 2024

Accepted: 22 July 2025

Published online: 02 August 2025

 Check for updates

Shinsuke Nirengi^{1,2,3,4}, Benjamin Buck^{1,5}, Devleena Das^{1,6}, Carmem Peres Valgas da Silva^{1,3}, Jazmin Calyeca ^{1,7}, Lisa A. Baer^{1,2,3}, Hsiang-Ling Huang ^{1,3}, Pablo Vidal ^{1,2,3}, Revati S. Dewal^{1,3}, Kelsey M. Pinckard^{1,3}, Elisa Félix-Soriano^{1,2,3}, Diego Hernandez-Saavedra ^{1,3}, Andrew Gereá^{1,2,3}, Kavya Dathathreya^{1,6}, Silvia Duarte-Sanmiguel^{1,6}, Ty A. Saldana¹, Harrison L. Hookfin^{1,8}, Matthew W. Gorr^{1,8}, Valerie Bussberg⁹, Juan J. Aristizabal-Henao ⁹, Michael A. Kiebish⁹, Roeland J. W. Middelbeek ¹⁰, Laurie J. Goodyear ¹⁰, Paul M. Coen ¹¹, Krishna Chinthalapudi^{1,3}, Loren E. Wold ^{1,8}, Ana L. Mora ^{1,7}, Thomas J. Hund^{1,5,6}, Daniel Gallego-Perez^{1,2,6} & Kristin I. Stanford ^{1,2,3} ✉

Aging poses significant challenges to cardiovascular health necessitating novel therapeutic approaches. This study investigates the potential of the brown adipose tissue (BAT) derived lipokine 12,13-diHOME to mitigate age-induced impairments in cardiovascular function. Analysis of human and rodent plasma signaling lipids reveals a decline in 12,13-diHOME levels with age. Transplantation of BAT or sustained upregulation of 12,13-diHOME effectively preserved cardiac function in aged male and female mice. Bulk RNA-Seq of hearts from aged mice reveals significant increases in pathways involved in ER stress and fibrosis which were partially attenuated by BAT transplantation or sustained upregulation of 12,13-diHOME. Mechanistically, in vivo and in vitro models demonstrate that 12,13-diHOME alleviated ER stress through CaMKII inhibition, particularly in males. These findings underscore 12,13-diHOME as a promising candidate for combating age-related cardiovascular dysfunction, offering insights into potential therapeutic strategies for addressing cardiovascular diseases in aging populations.

Older adults are the fastest-growing demographic segment in the U.S. population and worldwide. It is predicted that more than 20% of the U.S. will be over the age of 65 by the year 2030¹. Aging is among the strongest risk factors for a multitude of diseases, including both metabolic and cardiovascular disease², elevating the significance of developing potential therapeutic treatments. Aging causes a decrease in systolic and diastolic cardiac function and an increase in pathological hypertrophy^{3,4}. These aging-induced effects on cardiovascular health and function are related to disrupted Ca²⁺ cycling, uptake, storage, and release⁵.

Aging is also associated with a decrease in brown adipose tissue (BAT), a tissue that plays an important role in combating the development of metabolic and cardiovascular disease^{6–10}. Recent epidemiological studies have established a positive correlation between BAT activity and cardiovascular function in humans^{10,11}. Studies in rodents have demonstrated that BAT transplantation, or BAT stimulation by cold or exercise stimulate the endocrine activity of BAT and affect whole-body metabolism and cardiovascular function^{12–15}. Previous work from our laboratory demonstrated that

BAT enhances calcium cycling and cardiac function in young, healthy, male mice, both in vivo and in vitro, via release of the lipokine 12,13-diHOME¹⁵⁶. However, the ability of BAT or 12,13-diHOME to directly affect cardiovascular health and function in a model of senescence has not been investigated.

In this study, we demonstrate that 12,13-diHOME is significantly decreased with age in both humans and rodents. Increasing 12,13-diHOME, either by BAT transplantation or sustained upregulation via tissue nanotransfection (TNT), preserves cardiovascular health and function in aged (~24 months old) male and female mice. Heart RNA-Seq data demonstrate an increase in the expression of genes involved in endoplasmic reticulum (ER) stress and the extracellular matrix with aging, which are attenuated by transplantation of BAT or an increase in 12,13-diHOME in male, but not female mice. Further, we identify a unique role for 12,13-diHOME to directly interact with and inhibit Ca^{2+} /calmodulin-dependent protein kinase II (CaMKII), identifying a potential mechanism for 12,13-diHOME to regulate Ca^{2+} cycling, a crucial factor that impairs cardiac function. Together, these data identify a role for BAT and 12,13-diHOME to prevent the age-induced decline in cardiac function.

Results

Circulating oxylipins are decreased with age in humans and mice While it is known that the thermogenic activity of BAT decreases with age^{6–10}, less is known about the effect of age on the endocrine function of BAT. To determine if circulating lipids were altered with age, we performed liquid chromatography mass spectrometry (LC-MS/MS) on plasma of young (aged 18–35) and aged (aged 65–90) human subjects. A panel of 88 mediator lipids with annotated signaling properties was detected. One-way hierarchical clustering (Fig. 1a) and principal component analysis (Fig. 1b) revealed a distinct effect of age on lipid signaling in humans. To probe age-induced changes in individual lipids, we performed differential expression analysis and focused on signaling lipids that changed on a Log2 fold scale with $p < 0.05$. Nineteen lipids were altered with age in humans; 9 decreased with age, and 10 increased with age (Fig. 1c).

The effect of age on signaling lipids was also measured in young (3-month-old) and aged (18-month-old) male mice. One-way hierarchical clustering and principal component analysis exposed a distinct effect of age on lipid signaling in mice (Fig. 1d, e). A volcano plot revealed 31 signaling lipids were decreased, and one signaling lipid increased, in aged mice (Fig. 1f). Interestingly, there were seven oxylipins that decreased with age in both mice and humans (Supplementary Table 1 and Supplementary Data 1, 2), including 12,13-diHOME (Fig. 1g, h), which we have previously identified to be released from BAT and improve cardiac function¹⁵.

Transplantation of BAT ameliorates age-induced impairments in cardiac function

To investigate whether the decrease in 12,13-diHOME contributes to age-related impairments in cardiac function, we increased BAT mass by transplantation^{13,15}. Our previous work demonstrated that BAT transplantation increases circulating 12,13-diHOME in young, male mice¹⁵. BAT was transplanted from young (3-month-old) male and female mice into the visceral cavity of sex-matched 21-month-old mice^{13,15} (Fig. 2a). Twelve weeks post-transplantation, echocardiography revealed that +BAT preserved ejection fraction in male and female mice (Fig. 2b) and attenuated the age-induced increase in left ventricular posterior wall thickness (LVPW) (Fig. 2c). Importantly, as cardiac hypertrophy is a hallmark of cardiac aging, the hypertrophy index (LVPW/diastolic diameter) was calculated in male and female mice. The hypertrophy index was significantly reduced in +BAT male and female mice (Fig. 2d and Supplementary Tables 2, 3). In vivo cardiac hemodynamics revealed that male and female +BAT had increased systolic function (Fig. 2e). A greater $-\text{dP}/\text{dt}_{\text{min}}$ in +BAT

mice indicated accelerated relaxation and enhanced diastolic function (Fig. 2f) compared to age- and sex-matched sham mice. There was no effect of BAT transplantation on body composition or glucose tolerance in aged male or female mice (Supplementary Fig. 1a–d). Together, these data demonstrate that +BAT counteracts age-induced cardiac dysfunction and pathological hypertrophy in both male and female mice.

The viability of transplanted BAT was assessed by 2-deoxy-D-glucose (2-DG) injection and gene expression analysis. Twelve weeks after BAT transplantation, 2-DG injection showed active glucose uptake by the transplanted BAT (Supplementary Video). Gene expression analysis revealed no differences in gene expression of *Ephx1*, or *Pgc1a* in endogenous BAT compared to transplanted BAT. *Ephx2*, *Prdm16*, *Ucp1*, and *Glut4* were still present in transplanted BAT, but expression was decreased in the transplanted tissue, similar to a previous study (Fig. 1e)¹³. There were also no changes in inflammatory markers of the endogenous pgWAT in mice that received +BAT compared to Sham (Supplementary Fig. 1f) mice.

To determine if this improvement in cardiovascular function was specific to transplantation of BAT, or if transplantation of adipose tissue from a young mouse would be sufficient to confer these beneficial effects, 0.1 g of perigonadal white adipose tissue (pgWAT) was transplanted from young (3-month-old) male mice into the visceral cavity of sex-matched 21-month-old mice^{12–15}. Transplantation of 0.1 g pgWAT did not affect ejection fraction (Supplementary Fig. 2a) or in vivo cardiac hemodynamics compared to Sham mice (Supplementary Fig. 2b, c). There were no changes in inflammatory markers of the endogenous pgWAT in mice that received +WAT compared to Sham (Supplementary Fig. 2e) mice. Taken together, these data indicate that the improvement in cardiovascular health and function is specific to transplantation of BAT.

BAT transplantation increases 12,13-diHOME in aged male and female mice

Given our data demonstrating the effect of age on signaling lipids, the putative endocrine role of BAT, and our previous studies demonstrating the effect of 12,13-diHOME on cardiovascular function, we performed LC-MS/MS on plasma from male and female Sham and +BAT mice to determine if increasing BAT altered the lipidomic profile of aged male and female mice. A volcano plot revealed that BAT transplantation in aged mice altered the levels of seven lipids: three were decreased and four were increased, including 12,13-diHOME (Fig. 3a, b and Supplementary Table 4). There was no increase in 12,13-diHOME in mice that received 0.1 g pgWAT compared to Sham mice (Supplementary Fig. 2e).

Acute injection of 12,13-diHOME treatment improves cardiac function in male aged mice

Since increasing BAT (+BAT) resulted in an increase in 12,13-diHOME, and 12,13-diHOME has previously been shown to increase cardiac function in young, male mice¹⁵, we investigated the role of 12,13-diHOME to mitigate age-induced impairments in cardiovascular function. Aged male and female mice were injected with 12,13-diHOME or an equivalent amount of its isomer, 9,10-diHOME, and in vivo cardiac hemodynamics were measured. Acute treatment with 12,13-diHOME increased systolic (Fig. 3c) and diastolic (Fig. 3d) function in male mice. Interestingly, these improvements were not observed in female mice (Supplementary Fig. 3a, b).

Sustained overexpression with 12,13-diHOME improves cardiac function in male and female aged mice

After determining the effect of 12,13-diHOME to acutely increase in vivo cardiac hemodynamics, we investigated the potential therapeutic applications of an increase in 12,13-diHOME. 12,13-diHOME,

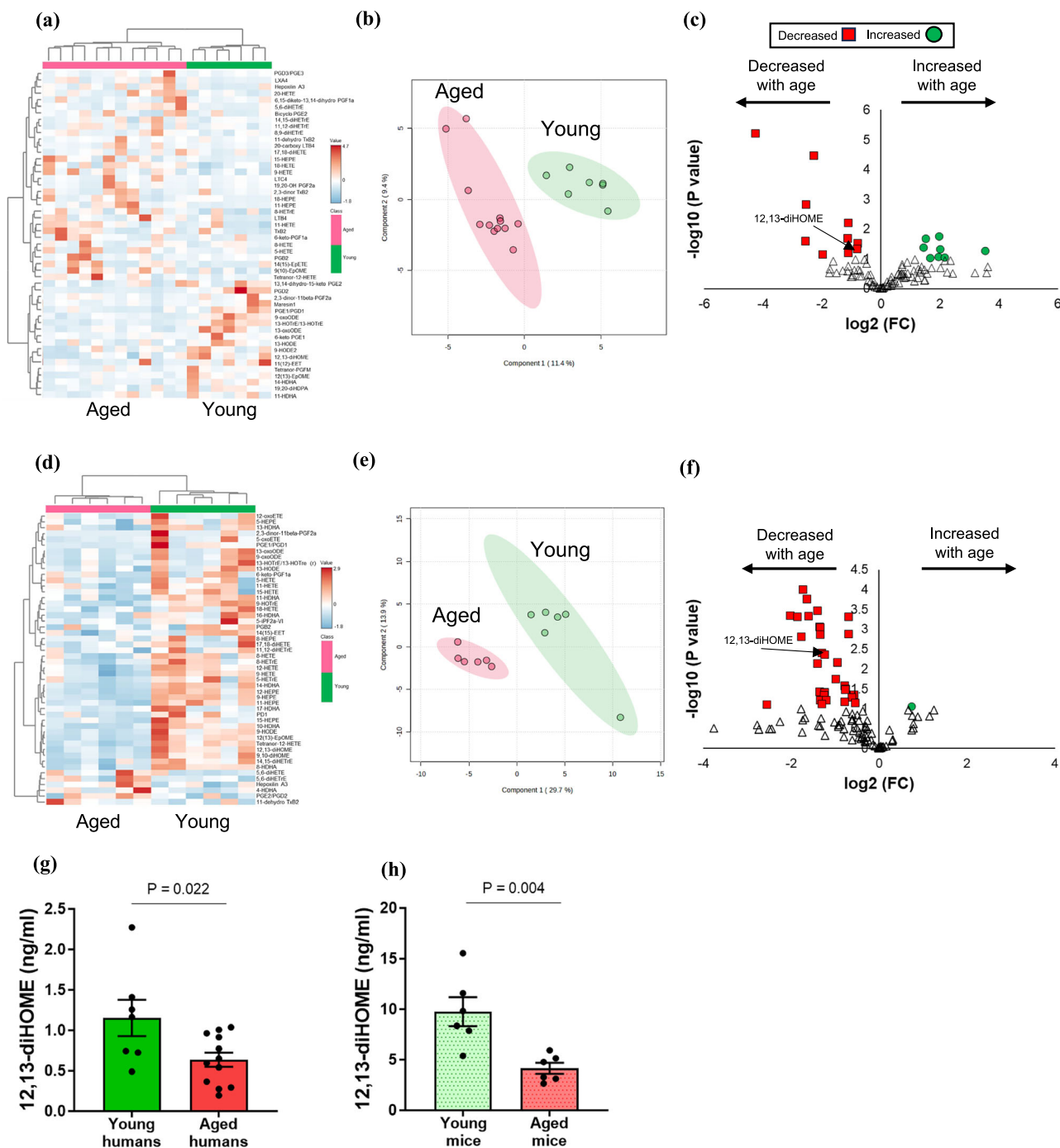


Fig. 1 | Circulating lipids are altered with age in humans and mice. Plasma lipid profiles of young (18–35 year old) and older (65–90 year old) humans displayed as **a** heat map, **b** principal component analysis, and **c** volcano plot. Plasma lipid profiles of young (3 months old) and older (24 months old) male mice displayed as **d** heat map, **e** principal component analysis, and **f** volcano plot. Quantification of 12,13-diHOME in **g** humans (green: young, red: aged) and **h** mice (dotted green: young, dotted red: aged). Humans $n = 7$ and 12 per group. Mice $n = 7$ per group. Data are expressed as mean \pm SEM. Volcano plot shows the \log_2 fold change versus $-\log_{10}(p)$ value from two-sided Student's t tests. False discovery rate (FDR) correction was applied, with significance threshold set at $FDR < 0.05$ (**c**, **f**). Two-tailed P values by unpaired Student's t test (**g**, **h**).

young, dotted red: aged). Humans $n = 7$ and 12 per group. Mice $n = 7$ per group. Data are expressed as mean \pm SEM. Volcano plot shows the \log_2 fold change versus $-\log_{10}(p)$ value from two-sided Student's t tests. False discovery rate (FDR) correction was applied, with significance threshold set at $FDR < 0.05$ (**c**, **f**). Two-tailed P values by unpaired Student's t test (**g**, **h**).

similar to other oxylipins, has a very short half-life^{16–20}; we found that 30 min after acute injection there is no difference in circulating 12,13-diHOME (Supplementary Fig. 4). To address the challenge posed by the short half-life of 12,13-diHOME, we utilized a non-viral gene therapy technology, TNT using plasmids that expressed genes of interest, Ephx1 and 2, the enzymes that convert 12,13-epOME to 12,13-diHOME^{12,14,15}. We have previously shown that a sustained overexpression of 12,13-diHOME via TNT preserved cardiac function in young, male mice¹⁵. To investigate if a sustained overexpression

of 12,13-diHOME preserved cardiac function in male and female mice in a model of aging, TNT was performed in 21-month-old mice using plasmids that contain the genes for the soluble epoxide hydrolase 1 and 2 (Ephx1 and Ephx2; TNT-Ephx1/2), or a Sham plasmid (TNT-Sham). These plasmids were electroporated on both the dorsal and ventral skin once a week for 6 weeks to drive sustained expression of Ephx1 and 2 (TNT-Ephx1/2) (Fig. 4a). TNT-driven overexpression of Ephx1/2 increased expression 12,13-diHOME in circulation (Fig. 4b, c; Supplementary Table 5) and

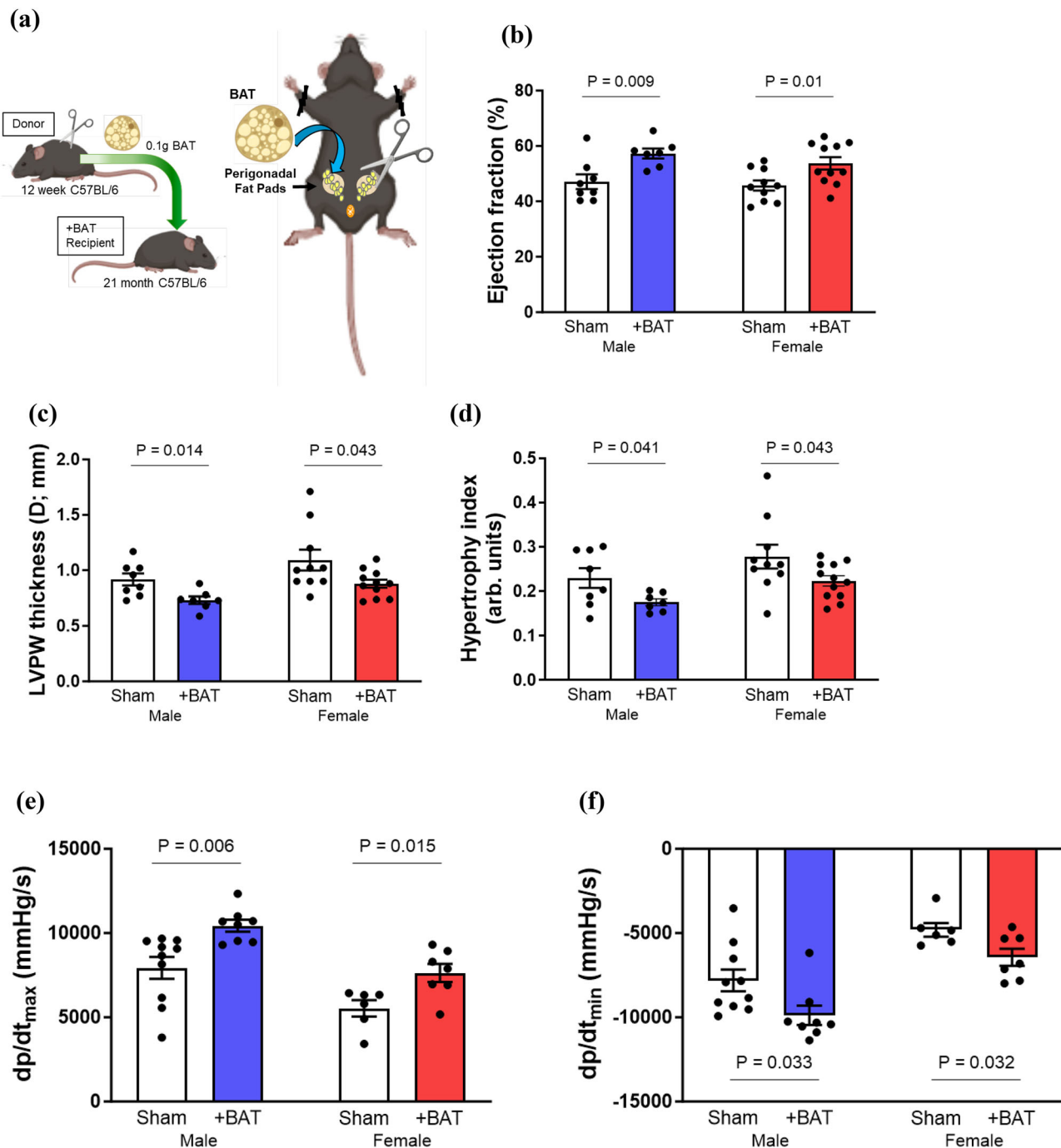


Fig. 2 | BAT transplantation improves cardiac function and remodeling in aged male and female mice. **a** Schematic illustration of BAT transplantation (Created in BioRender. Baer, L. (2025) <https://BioRender.com/0c6k2kp>); **b** Ejection fraction, **c** left ventricular posterior wall thickness (LVPW), **d** hypertrophy index and

e systolic and **f** diastolic function in aged male and female mice. $n = 8$ (sham males), $n = 7$ (+BAT males), $n = 10$ (sham females), $n = 11$ (+BAT females)-group. Data are expressed as mean \pm SEM. Two-tailed P values by unpaired Student's t test (**b–f**). Bar colors: white (sham), blue (+BAT males), red (+BAT females) (**b–f**).

expression of *Ephx1* and *Ephx2* in the skin (Fig. 4d). There was no effect of an increase in 12,13-diHOME on body composition or glucose tolerance (Supplementary Fig. 5a–d).

Similar to BAT transplantation (+BAT), treatment with TNT for 6 weeks preserved ejection fraction (Fig. 4e, Supplementary Table 6,7), LVPW thickness (Fig. 4f), and reduced the hypertrophy index (Fig. 4g). Male and female mice and TNT-Ephx1/2 increased systolic and diastolic function compared to sex-matched TNT-Sham mice (Fig. 4h, i). Together, these data indicate that TNT-driven up-regulation of 12,13-diHOME preserves cardiovascular health and function in male and female aged mice.

Increasing BAT reduces markers of ER stress in hearts from aged mice

To decipher the underlying mechanisms through which +BAT or 12,13-diHOME attenuate the aging-induced changes in the heart, we investigated changes to the heart transcriptome by measuring bulk RNA Sequencing (RNA-Seq) in young (3 months of age), aged (24 months of age) and +BAT aged (24 months of age) male mice. Among the 13,807 genes detected, 143 genes were altered with age (100 increased and 43 decreased; young vs. aged) and 416 with +BAT (279 increased and 137 decreased; aged vs. +BAT aged) (Fig. 5a; Supplementary Fig. 6a,b). Differential gene expression analysis revealed certain gene clusters

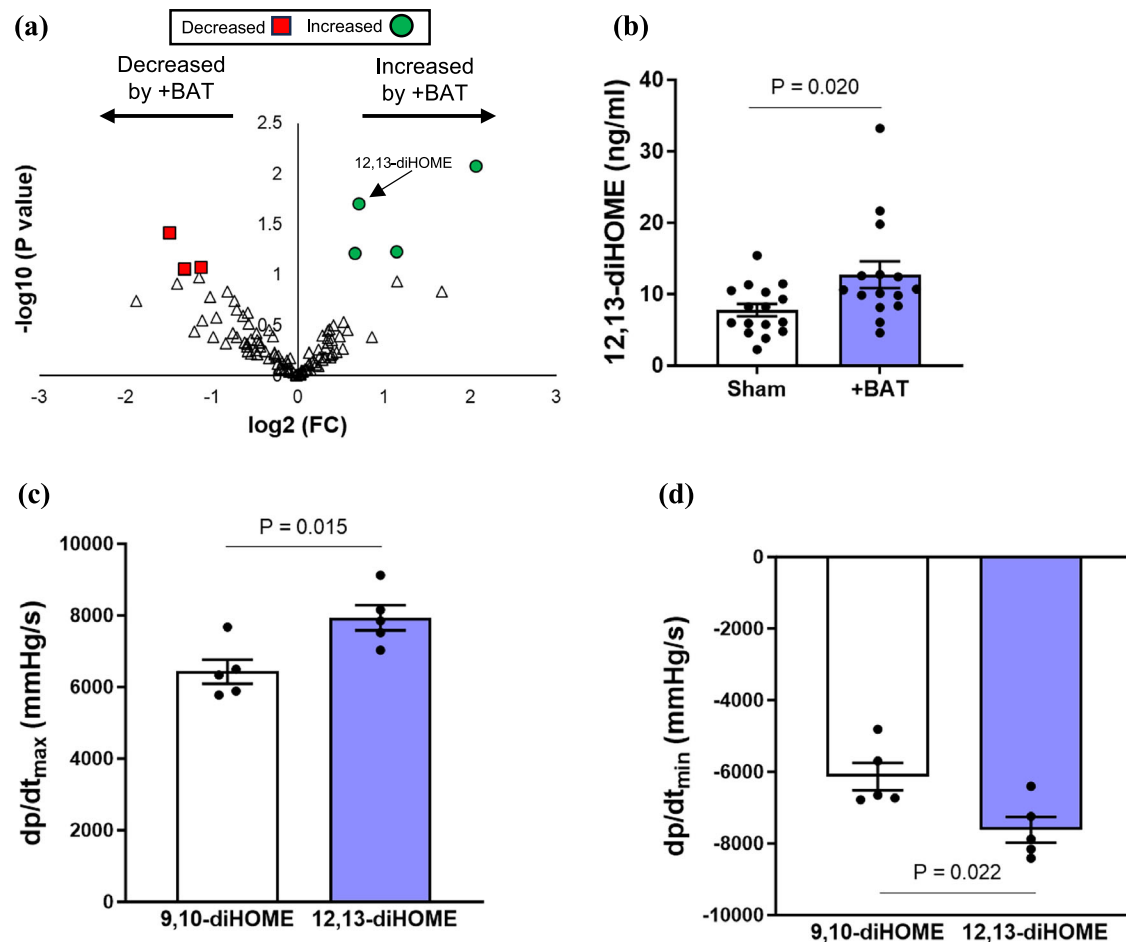


Fig. 3 | BAT transplantation increases 12,13-diHOME and injection with 12,13-diHOME improves cardiac function. **a** Volcano plot of lipidomics; $n = 16$ (sham), $n = 15$ (+BAT), and **b** quantification of 12,13-diHOME after BAT transplantation. Acute injection of 12,13-diHOME increases **c** systolic and **d** diastolic function in aged male mice. $n = 4$ (9,10-diHOME) and 5 (12,13-diHOME). Data are expressed as

mean \pm SEM. Volcano plot shows the log2 fold change versus $-\log_{10}(p)$ value from two-sided Student's t tests. False discovery rate (FDR) correction was applied, with significance threshold set at $FDR < 0.05$ (**a**). Two-tailed P values by unpaired Student's t test (**b–d**). Bar colors: white (9,10-diHOME), blue (12,13-diHOME) (**b–d**).

(cluster 2, 4, and 8) that were altered in a similar manner in the +BAT and young mice as observed in the heatmap (Fig. 5a). To characterize the mechanism of how +BAT affects the aged heart, Gene Ontology (GO) analysis detected changes in pathways involved in the extracellular matrix, mitochondria, and ER in both aging and +BAT conditions (Fig. 5b, c).

BAT and 12,13-diHOME reduce ER stress and perivascular fibrosis in an aged male, but not female mice

It is well established that ER stress is a pivotal factor in aging, as it can induce mitochondrial dysfunction and hypertrophy of the extracellular matrix. We first validated our RNA-Seq results by measuring gene expression via qPCR in genes involved in ER stress with aging that were reverted to a “young” phenotype by BAT transplantation. In line with the RNA-seq data, genes involved in ER stress were increased in aged male mice compared to young mice, and this was completely attenuated in the +BAT aged mice (Fig. 6a). To investigate changes in ER stress genes more quantitatively, we measured the ratio of the spliced isoform to total XBP1 mRNA which can be used as a marker of the IRE1-mediated ER stress response²¹. There was a decrease in spliced to unspliced XBP1 ratio in young and +BAT aged mice compared to sham mice, indicating an attenuation of ER stress with +BAT (Fig. 6b). Interestingly, there was no difference in ER stress markers in female mice among young, aged, or +BAT aged (Supplementary Fig. 7a,b).

To determine if an increase in 12,13-diHOME attenuated the elevated expression of genes involved in ER stress, we measured markers of ER stress in TNT-Sham and TNT-Ephx1/2 male and female mice. Similar to what was observed with BAT transplantation (+BAT), TNT-Ephx1/2 significantly reduced expression of genes involved in ER stress compared to aged male mice. Furthermore, ER-stress-related apoptosis markers (GADD34 and Chop) were attenuated by the increase in 12,13-diHOME (Fig. 6c), and there was a decrease in spliced to unspliced XBP1 ratio in the TNT-Ephx1/2 mice compared to the TNT-Sham mice (Fig. 6d). Importantly, 30 min after injection with 12,13-diHOME, the sXBP1/uXBP1 ratio was significantly decreased in male mice, while there was no effect after injection of 9,10-diHOME (Fig. 6e). Interestingly, this reduction in ER stress was independent of other changes in cardiac inflammation (IL-6, IL-1 β , TGF- β , and TNF- α) and oxidative stress (SOD1, SOD2, Nrf2, and Gpx1) in aged males (Supplementary Fig. 8), suggesting the ER stress specific response.

In contrast to male mice, there were no differences in ER stress markers in female mice in response to TNT-Ephx1/2 (Supplementary Fig. 7b,c) or acute treatment of 12,13-diHOME (Supplementary Fig. 7d). After observing the lack of effect of 12,13-diHOME on ER stress in aged female mice, we compared the sXBP1/uXBP1 ratio in male and female mice. Consistent with previous literature²², female mice had a decreased sXBP1/uXBP1 ratio compared to male mice, indicating reduced ER stress (Supplementary Fig. 7e). Thus, it is

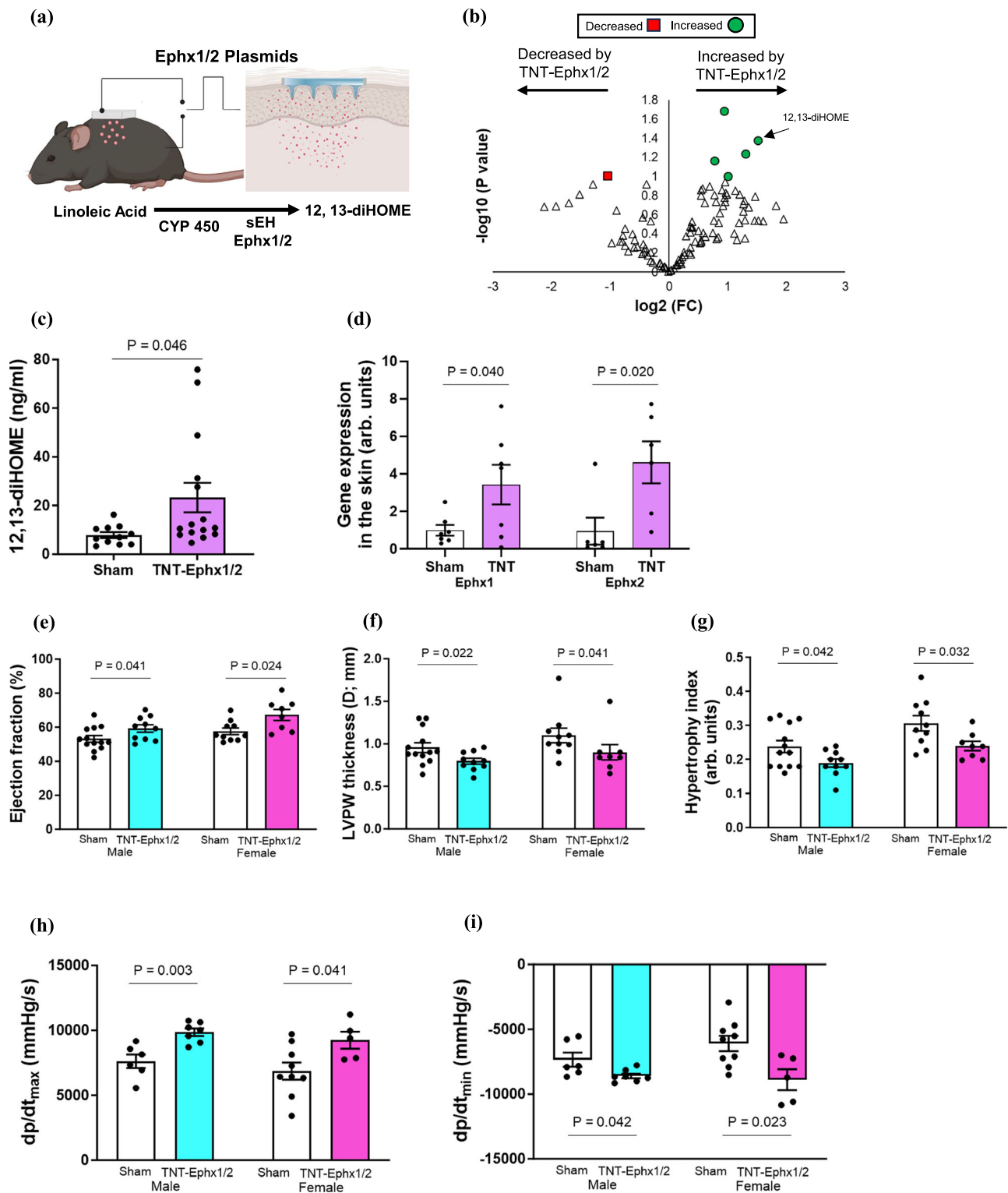


Fig. 4 | Sustained overexpression of 12,13-diHOME improves cardiac function and remodeling in aged mice. **a** Schematic illustration of tissue nano-transfection (TNT)- epoxide hydrolase 1 and 2 (Ephx1/2) intervention (Created in BioRender. Baer, L. (2025) <https://BioRender.com/Oc6k2kp>). **b** Volcano plot of signaling lipids, **c** quantification of 12,13-diHOME; $n = 12$ (sham) and $n = 15$ (TNT), and **d** TNT-Ephx1/2 increased gene expression of Ephx1 and 2 in the skin; $n = 7$ (sham) and $n = 6$ (TNT). **e** Ejection fraction, **f** left ventricular posterior wall thickness (LVPW), **g** hypertrophy index; $n = 13$ (sham males), $n = 7$

(TNT males), $n = 10$ (sham females), $n = 8$ (TNT females), **h** systolic function, and **i** diastolic function in aged mice; $n = 6$ (sham males), $n = 7$ (TNT males), $n = 9$ (sham females), $n = 5$ (TNT females). Data are expressed as mean \pm SEM. Volcano plot shows the log₂ fold change versus -log₁₀(p) value from two-sided Student's t tests. False discovery rate (FDR) correction was applied, with significance threshold set at $FDR < 0.05$ (**b**). Two-tailed P values by unpaired Student's t test (**c**–**i**). Bar colors: white (sham), purple (TNT) (**c**, **d**). Bar colors: white (sham), blue (TNT males), pink (TNT females) (**e**, **i**).

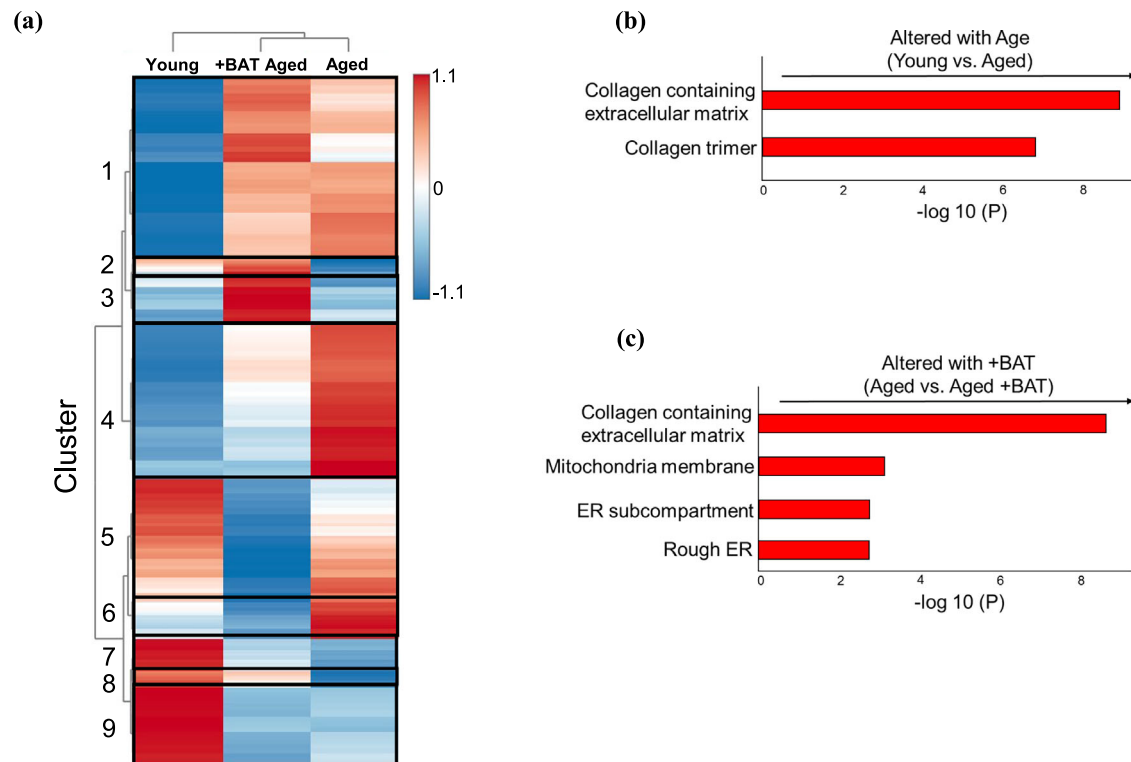


Fig. 5 | BAT transplantation alters pathways involved in ER stress and fibrosis in the heart. a Heat maps comparing young (3 months old), aged (24 months old) and +BAT aged male mice. **b, c** Gene ontology analysis of pathways altered among young (3 months old; $n = 7$), aged (24 months old; $n = 9$) and +BAT aged male mice

($n = 5$). Gene ontology enrichment analysis was performed using Metascape. P -values were calculated using the cumulative hypergeometric test and adjusted for multiple comparisons using the Benjamini-Hochberg method (**b, c**).

possible that there is no effect of 12,13-diHOME to reduce ER stress in female mice because their baseline ER stress is already lower than that of male mice.

RNA-Seq analysis also revealed significant increases in extracellular matrix (ECM) pathways with +BAT. Considering the important biological role of fibroblasts in the production of the ECM, and the fact that perivascular fibrosis is known to increase with age²³, we investigated if an increase in 12,13-diHOME affected perivascular fibrosis in male mice. Perivascular fibrosis and wall lumen ratio were both reduced in +BAT aged compared to sham, and in TNT-Ephx1/2 mice compared to TNT-Sham (Fig. 6f, g). The tunicamycin-induced spliced to unspliced XBP1 ratio was attenuated by 12,13-diHOME in cardiac fibroblasts from young male mice (Fig. 6h). Together, these data indicate that an increase in 12,13-diHOME through either BAT transplantation or TNT negates aging-induced increases in ER stress and perivascular fibrosis in male mice.

12,13-diHOME does not improve cardiac function or mediate ER stress in $n\text{NOS}^{-/-}$ male mice

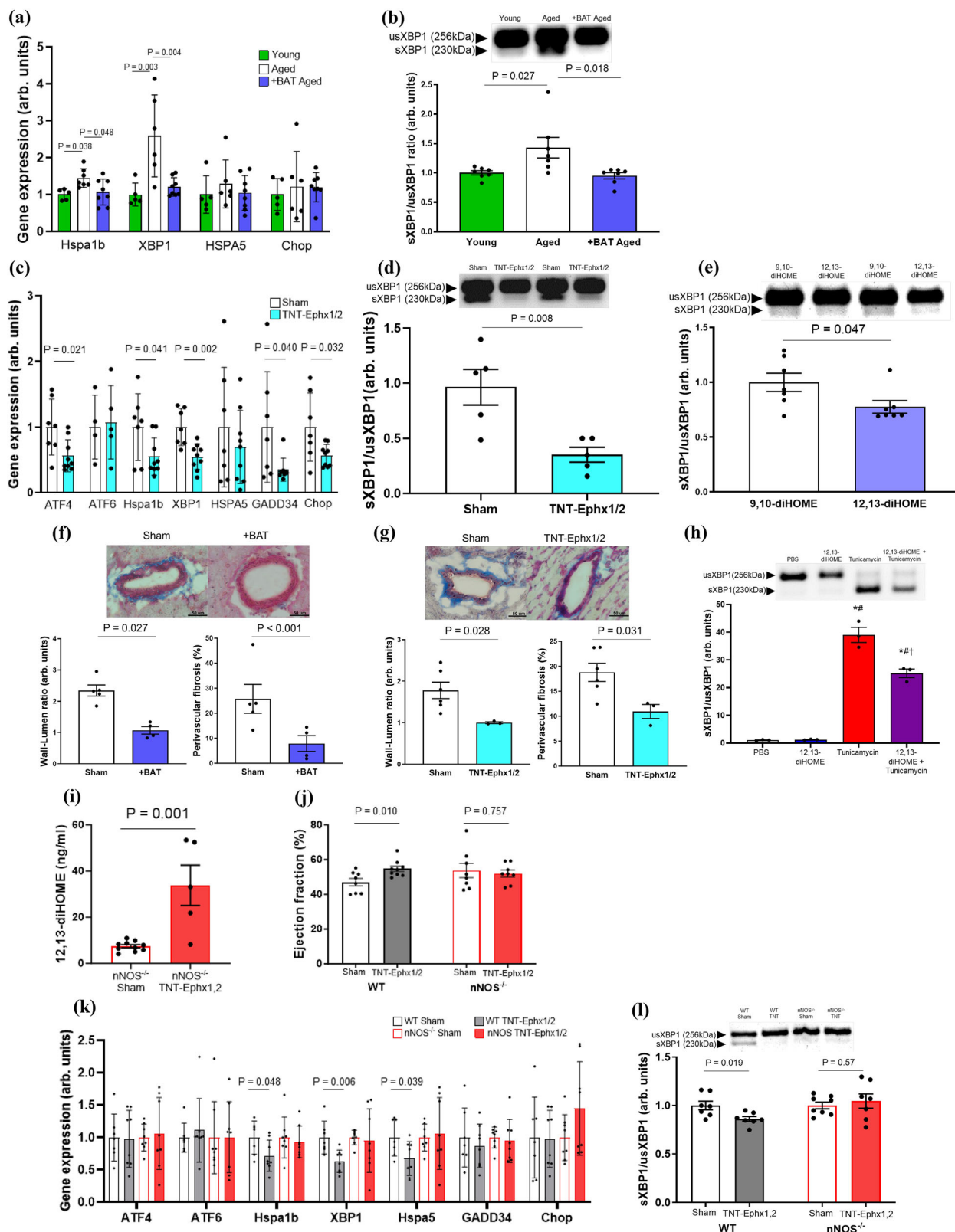
Our previous studies showed that 12,13-diHOME requires nNOS to exert its beneficial effects on cardiac function in both in vivo and in vitro¹⁵. Consequently, we investigated TNT-Ephx1/2 could attenuate ER stress and improve cardiac function in $n\text{NOS}^{-/-}$ mice, where 12,13-diHOME is increased but cannot exert its beneficial effects. It is established that a high-fat diet can increase markers of ER stress²⁴, thus wild-type (WT) and $n\text{NOS}^{-/-}$ were placed on a high-fat diet (60% kcal from fat) beginning at 6 weeks of age. At 12 weeks of age, mice were subjected to TNT-Ephx1/2 for 6 weeks. TNT-Ephx1/2 increased 12,13-diHOME in circulation in $n\text{NOS}^{-/-}$ mice (Fig. 6i). While the $n\text{NOS}^{-/-}$ mice weighed less than the WT mice, there was no effect of an increase in 12,13-diHOME on body weight, % fat mass, or % lean mass (Supplementary Fig. 9a-c). There was no effect of an increase in 12,13-diHOME

on glucose tolerance, similar to our previous studies^{12,14,15} (Supplementary Fig. 9d).

We then investigated the effects of an increase in 12,13-diHOME on cardiovascular function in WT and $n\text{NOS}^{-/-}$ mice fed a high-fat diet. Ejection fraction was preserved in WT TNT-Ephx1/2 mice compared to WT TNT-Sham mice, but there was no effect of TNT-Ephx1/2 to affect ejection fraction or other cardiovascular parameters in $n\text{NOS}^{-/-}$ mice (Fig. 6j, Supplementary Table 8). To determine if this preservation of ejection fraction was related to changes in ER stress genes, a panel of ER stress genes was measured and revealed that TNT-Ephx1/2 reduced markers of ER stress in WT mice but had no effect in $n\text{NOS}^{-/-}$ mice (Fig. 6k). There was also a decrease in spliced to unspliced XBP1 ratio in the WT TNT-Ephx1/2 mice compared to the WT TNT-Sham mice, while this was not altered in the $n\text{NOS}^{-/-}$ mice (Fig. 6l). Collectively, these data indicate that TNT-Ephx1/2 does not affect cardiac function in the $n\text{NOS}^{-/-}$ mice, indicating that the improvement in cardiac function is specifically mediated by 12,13-diHOME.

12,13-diHOME mediates ER stress by attenuation of pCaMKII

Age-induced increases in ER stress are attributed to disrupted calcium homeostasis^{25,26}. CaMKII is a key player in cardiac dysfunction and pathological remodeling of the heart and acts as a pathological mediator of ER stress, and aging increases CaMKII activity in the heart²⁷⁻³¹. To determine if 12,13-diHOME mediates ER stress by modulating CaMKII signaling, we measured the levels of total CaMKII and CaMKII phosphorylated at T286/287 (pCaMKII) in the hearts of mice with increased 12,13-diHOME. These measurements served as in situ surrogates for CaMKII activity and revealed that sustained overexpression of 12,13-diHOME reduced pCaMKII in male (Fig. 7a), but not female mice (Supplementary Fig. 10a). Overexpression of 12,13-diHOME attenuated pCaMKII in high-fat diet-fed, young, WT mice, but not in $n\text{NOS}^{-/-}$ male mice (Fig. 7b).



To determine if there was a direct interaction of 12,13-diHOME and CaMKII, we performed *in vitro* experiments using commercially available purified components of 12,13-diHOME and CaMKII δ protein, which showed that 12,13-diHOME directly inhibits CaMKII activity at micromolar concentrations (Fig. 7c). Microscale Thermophoresis (MST) studies indicated that 12,13-diHOME binds directly to CaMKII δ \pm ATP with a K_d of 19 and 24 μ M in the absence and presence of ATP,

respectively. These experiments suggest that 12,13-diHOME allosterically interacts with CaMKII δ rather than competing for the kinase active site (Fig. 7d, e).

In order to determine if 12,13-diHOME could reach a concentration *in vivo* that directly inhibit pCaMKII, we measured pCaMKII after acute injection of 12,13-diHOME in the heart and showed that injection of 12,13-diHOME, but not 9,10-diHOME, significantly reduced pCaMKII

Fig. 6 | 12,13-diHOME attenuates age-induced ER stress in male mice. a, b BAT transplantation attenuates ER stress in the hearts of aged mice; $n = 5$ (Young; green bar), $n = 7$ (aged; white bars), $n = 8$ (+BAT aged; blue bars). **c, d** TNT-Ephx1/2 reduces ER stress in the hearts of aged mice; $n = 7$ (sham; white bars), $n = 8$ (TNT; light blue bars). **e** Acute treatment with 12,13-diHOME (12,13-diHOME; blue bars; $n = 7$) attenuates ER stress compared to vehicle (9,10-diHOME; white bars; $n = 7$). **f** BAT transplantation ($n = 5$; blue bars) and **g** TNT-Ephx1/2 ($n = 3$; light blue bars) reduce perivascular fibrosis and wall-to-lumen ratio compared to sham controls ($n = 3$ or 5; white bar). Scale bar, 50 μm (black). **h** usXBP1/sXBP1 ratio in murine fibroblasts after incubation with tunicamycin and/or 12,13-diHOME; $n = 3$. Bar colors: white (PBS), blue (12,13-diHOME), red (Tunicamycin), purple (12,13-diHOME +

Tunicamycin). $P < 0.001$ vs. PBS; $^{\#}P < 0.001$ vs. 12,13-diHOME; $^{\dagger}P < 0.001$ vs. Tunicamycin. **i** 12,13-diHOME; $n = 10$ (sham; white), $n = 5$ (TNT; red), **j** ejection fraction, **k** expression of ER stress in the heart; $n = 8$ or 9, and **l** PCR of usXBP1/sXBP1 ratio in the heart; TNT-Sham ($n = 7$; white bars) or TNT-Ephx1/2 ($n = 7$; gray bars) in young WT and TNT-Sham ($n = 7$; open red bars) or TNT-Ephx1/2 ($n = 7$; red bar) in nNOS $^{-/-}$ male mice fed a high-fat diet. $P < 0.05$ vs. Sham. Data are expressed as mean \pm SEM (**b, d, e, f, g–j, l**) or mean \pm SD (**a, c, k**). Statistical analysis was performed using two-way ANOVA with Tukey's multiple comparisons test **a, b, h** or unpaired two-tailed Student's t test (**c–g, i–l**). Imaging data in (**f**) and (**g**) were obtained from three independent cohorts.

in the hearts of mice (Fig. 7g). Importantly, after acute injection, the concentration of 12,13-diHOME in the heart was ~ 200 ng/g of tissue, which equates to a concentration 2–3 orders of magnitude higher than levels measured in the circulation (in the micromolar range) and sufficient to inhibit CaMKII in the heart (Fig. 7f).

There was no effect of 12,13-diHOME to reduce pCaMKII in female mice (Supplementary Fig. 10b). Interestingly, we found that baseline pCaMKII was reduced in aged female mice compared to aged male mice (Supplementary Fig. 11c), indicating this could be a potential reason for the lack of effect.

As there was a direct effect of 12,13-diHOME to inhibit CaMKII activity, we investigated if 12,13-diHOME could modulate the detrimental effects induced by hyperactive CaMKII, including ER stress and mitochondrial dysfunction. Accordingly, we subjected isolated primary murine fibroblasts to hyperphosphorylating conditions using okadaic acid (OA) and Angiotensin II (AT2)³². Incubation with AT2 and OA reduced mitochondrial respiration and increased ER stress, while incubation with 12,13-diHOME restored mitochondrial respiration and attenuated ER stress (Fig. 7h–j). To investigate the translational relevance of this observation, we repeated the experiments using human fibroblasts. Similar to the murine cells, incubation with OA and AT2 reduced respiration in primary human fibroblasts and this was partially negated upon incubation with 12,13-diHOME (Fig. 7k, l). Together, these data provide a mechanism for 12,13-diHOME to modulate CaMKII activity and ER stress in a model of aging.

Discussion

Aging is a major risk factor for the development of cardiovascular disease^{33–36}. In this study, we identified a mechanism for BAT and 12,13-diHOME to attenuate the effects of age on cardiovascular health and function. We demonstrate that increasing BAT or 12,13-diHOME preserved cardiovascular health and function in male and female mice. In male mice, 12,13-diHOME attenuated the expression of genes involved in ER stress and hyperphosphorylation of CaMKII, identifying a pathway for 12,13-diHOME to regulate cardiovascular health and function.

Recent studies have identified the multifaceted roles of BAT, including its endocrine functions^{15,37–39}, potentially contributing to the amelioration of age-related metabolic diseases. Our study expands upon this by revealing the effects of age to alter the signaling lipidome in mice and humans. Notably, while it is well known that BAT mass and thermogenic activity are decreased with age^{6–10}, these data suggest that the endocrine function of BAT also decreases with age as BAT-released oxylipins, and specifically 12,13-diHOME, were decreased with age in humans and mice. Remarkably, this study demonstrates a role for BAT transplantation or an increase in 12,13-diHOME to increase cardiac function, thus negating the effects of aging on the heart. While BAT secretes several endocrine factors in addition to 12,13-diHOME that have beneficial effects on the heart, such as FGF21, IL-6, miRNAs (miR-125b-5p, miR-128-3p, and miR-30d-5p), and other oxylipins^{13,15,37–40}, our previous study reported that treatment with sEH inhibitors prevented the beneficial effects BAT transplantation on cardiac function^{13,15,39}. These data also emphasize the role for 12,13-diHOME to function as a mediator

in the crosstalk among BAT and the heart^{15,37–40}. In addition, while we did not see an effect of transplantation of WAT to increase cardiac function or increase 12,13-diHOME, in the absence of a direct comparison of Sham, +BAT, and +WAT mice with a comparable n , it cannot be definitively excluded that 12,13-diHOME is not increased following WAT transplantation. This is a limitation of the current study.

There is significant data demonstrating the physiological function of oxylipins⁴¹ and the beneficial effects of 12,13-diHOME^{12,14,15}. Male and female patients with cardiovascular disease have significantly reduced circulating 12,13-diHOME compared to healthy individuals of the same age¹⁵. However, because it has a very short half-life^{16–20}, the therapeutic potential of 12,13-diHOME has not been thoroughly exploited. To circumvent this issue, we developed a paradigm-shifting approach to induce a sustained systemic up-regulation of 12,13-diHOME via TNT⁴² in the skin. The use of TNT successfully and consistently increases circulating 12,13-diHOME, allowing us a novel method to test its therapeutic potential and mechanistically determine how it is functioning to regulate cardiovascular health and function.

ER stress increases with age^{25,26}. Excessive ER stress is a key contributor to the adverse effects of impaired cardiac function through various pathogenic reactions, including cardiac dysfunction, mitochondrial dysfunction, Ca²⁺ dysregulation, fibrosis, and apoptosis^{43–47}. In male mice, this correlates with impaired Ca²⁺ homeostasis^{25,26}. Our prior investigation demonstrated a pivotal role of 12,13-diHOME in modulating Ca²⁺ homeostasis in isolated cardiomyocytes from wild-type (WT) mice¹⁵, but ER stress was not investigated as a mechanism to mediate this effect. In the present study, RNA-Seq data revealed an increase in genes involved in ER stress with age that was attenuated by BAT transplantation. Both BAT transplantation and a sustained over-expression of 12,13-diHOME using TNT-Ephx1/2 decreased the expression of genes involved in ER stress in male, but not female mice. Importantly, ER stress genes were not increased with age in the hearts of female mice, suggesting that 12,13-diHOME or BAT may increase cardiac function in female mice via a different mechanism.

CaMKII is a key player in cardiac dysfunction and pathological remodeling of the heart. It is activated by a broad range of stress stimuli, including Ca²⁺ and acts as a pathological mediator of ER stress. CaMKII activity is increased in the heart with age, and previous studies have investigated the role of CaMKII and ER stress in models of aging and cardiovascular disease. In these data, we identified a direct role for 12,13-diHOME to act as an allosteric inhibitor of CaMKII with the ability to attenuate pCaMKII, both in vivo and in vitro. The K_d for 12,13-diHOME/CaMKII interaction was found to be in the range of 19–24 μM . It is important to note that while the concentration of circulating 12,13-diHOME is in the nanomolar range, this may be due to its short half-life, which is influenced by metabolic processes, including beta-oxidation and enzymatic clearance^{16–20}. Indeed, our acute 12,13-diHOME treatment data show that while pCaMKII is decreased, the circulating levels did not change. However, the concentration of 12,13-diHOME in the heart after acute injection is in the range of the K_d measured. These data provide mechanistic insight into the role of 12,13-diHOME to mediate cardiovascular function in males.

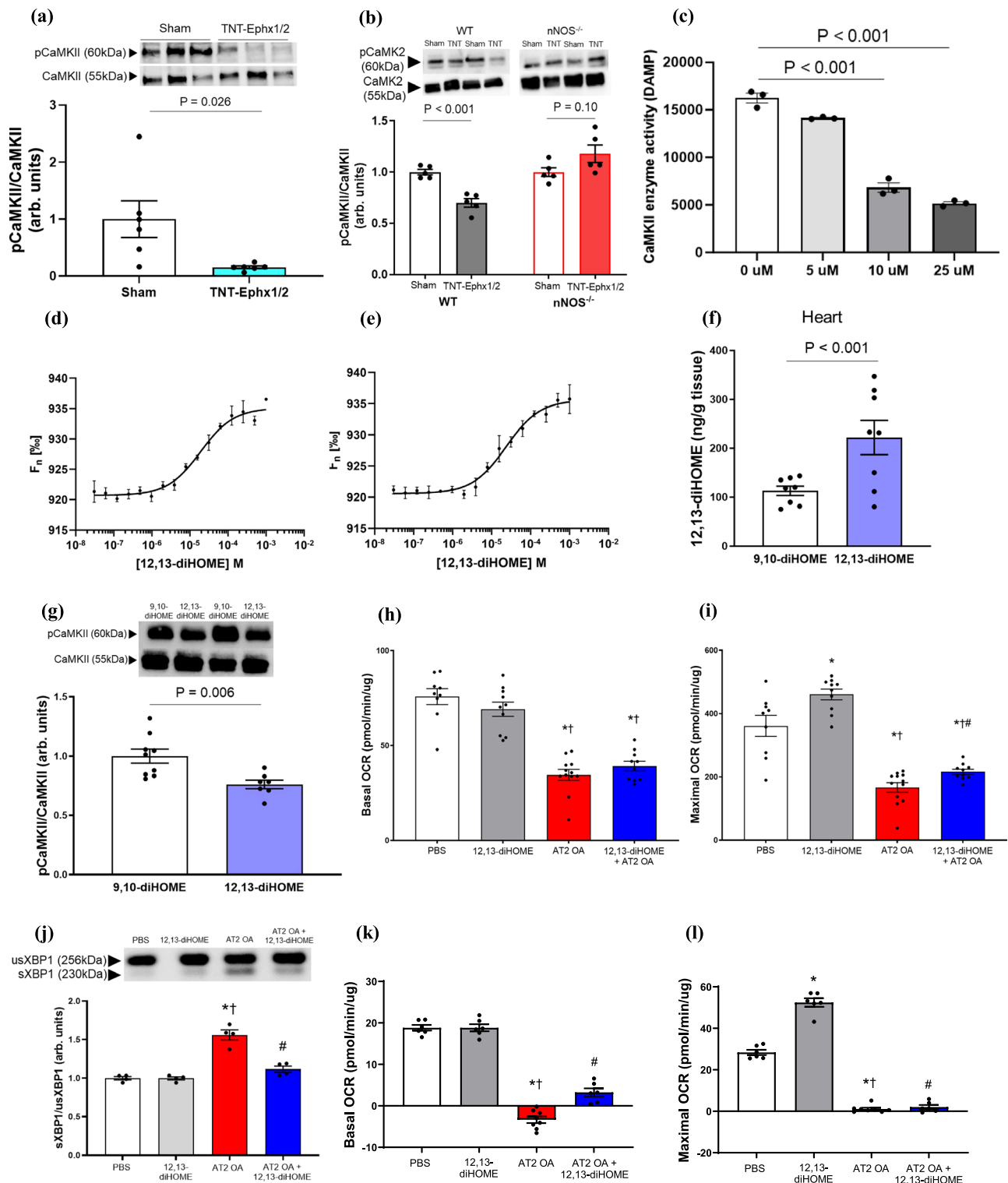


Fig. 7 | 12,13-diHOME attenuates CaMKII activity. **a** Phosphorylated CaMKII (pCaMKII) levels are significantly reduced in aged mouse hearts following TNT-Ephx1/2 treatment compared to sham controls (white bar, $n = 6$; TNT, light blue bar, $n = 6$). **b** In WT mice on a high-fat diet, TNT-Ephx1/2 lowers pCaMKII expression, an effect absent in nNOS^{-/-} mice. Bar colors: white (WT Sham; $n = 5$), gray (WT TNT; $n = 5$), open red (nNOS^{-/-} Sham; $n = 5$), red (nNOS^{-/-} TNT; $n = 5$). **c** In vitro CaMKII activity assay after 5-min incubation with 12,13-diHOME (0–25 μ M) and [³²P] (2.5 μ Ci) in 100 μ L reaction buffer (~800 μ g CaMKII). Bar colors: white (0 μ M), light to dark gray (5–25 μ M). **d, e** MST analysis shows direct binding of 12,13-diHOME to CaMKIIδ with $K_d = 19.1 \mu$ M (no ATP) and 23.7 μ M (with ATP). **f** Acute 12,13-diHOME treatment (blue bar, $n = 8$) raises cardiac levels vs. 9,10-diHOME (white bar, $n = 8$),

g and reduces pCaMKII levels. **h, i** Basal and maximal oxygen consumption rates (OCR) in human fibroblasts. Bar colors: white (PBS, $n = 9$), gray (12,13-diHOME, $n = 10$), red (AT2 + OA, $n = 12$), purple (12,13-diHOME + AT2 + OA, $n = 10$). $^*P < 0.001$ vs. PBS; $^{\dagger}P < 0.001$ vs. 12,13-diHOME; $^{\#}P < 0.001$ vs. AT2 + OA. **j** usXBP1/sXBP1 ratio in murine fibroblasts after treatment with OA, AT2, and 12,13-diHOME. $^*P < 0.001$ vs. PBS; $^{\dagger}P < 0.001$ vs. 12,13-diHOME; $^{\#}P < 0.001$ vs. AT2 + OA. **k, l** Basal and maximal OCR in human fibroblasts. Bar colors: white (PBS, $n = 6$), gray (12,13-diHOME, $n = 6$), red (AT2 + OA, $n = 8$), blue (12,13-diHOME + AT2 + OA, $n = 6$). Data are expressed as mean \pm SEM. Two-way ANOVA with Tukey's test **c, h–l**; unpaired two-tailed t test (**a, b, f, g**). Imaging data in (**f**) and (**g**) were obtained from three independent cohorts.

We observed similar cardiac phenotypes between males and females after BAT transplantation or TNT-Ephx1/2, however, the mechanism by which 12,13-diHOME improves heart function may be different among sexes. Our data show that TNT-Ephx1/2 attenuates pCaMKII and the ER stress in males, but not in females. The reason females did not exhibit lower pCaMKII levels with TNT-Ephx1/2 is not fully understood; one possible explanation is that females have lower baseline levels of pCaMKII. Evidence suggests that pCaMKII levels differ by sex, with the thoracic aortic constriction model increasing pCaMKII in males but not in females²². Our data also indicate that pCaMKII and sXBP1 levels are lower in aged females compared to aged males (Supplementary Fig. 7f and Supplementary 10c). Additionally, 12,13-diHOME enhances Ca^{2+} cycling and mitochondrial respiration in young cardiomyocytes¹⁵, both essential for heart function. Further studies are needed to investigate these aspects in aged females.

In conclusion, the findings of this study provide mechanisms and interactions to treat age-related cardiovascular dysfunction using BAT or 12,13-diHOME. While increasing BAT or 12,13-diHOME increased cardiac function in both male and female mice, the mechanism for these improvements are sex-specific. Future studies should delve into the underlying mechanisms contributing to sex-specific variations, enabling the development of personalized therapeutic approaches.

Methods

Human subjects

All participants provided written informed consent and the study protocol was approved by the Institutional Review Boards at Florida Hospital (IRBnet# 554559-144) or the Joslin Diabetes Center (IRB# 2015-11). Participants were divided into Young (age: 18–35 years, $n = 6$) and Aged (age: 65–90 years, $n = 12$). Exclusion criteria included inability or unwillingness to comply with the protocol, clinically significant cardiovascular disease including MI within the past year, the presence of peripheral vascular disease, hepatic disease, renal disease, muscular or neuromuscular disease, hematologic/oncologic disease, peripheral neuropathy, orthopedic limitations, history of pulmonary emboli, history of alcohol or substance abuse, current use of blood thinners or any medication that can alter glucose homeostasis.

Mouse model

All the mouse experiments in this study were conducted in accordance with the ARRIVE guidelines and were approved by the Institutional Animal Use and Care Committee at The Ohio State University. We purchased C57BL/6 male and female young (12 weeks old) (Charles River Laboratories), C57BL/6 male and female mice aged mice (18 months) (National Institutes of Health), and $\text{nNOS}^{-/-}$ male mice (B6;129S4-*Nos1^{tm1Pth}*/J; stock No. 002633; Jackson Labs). Mice had free access to food and water, were housed at 23 °C with a standard 12 h light/12 h dark cycle, and were randomly assigned to experimental groups for use in the experiments. Blinding was not performed during the conduct of the experiment or outcome assessment due to the nature of the study. All procedures and assessments were conducted by the same trained investigator.

Transplantation of BAT or pgWAT

We used established methods for BAT or pgWAT transplantation^{13,15,48–50}. Transplantation of 0.1 mg of interscapular BAT or pgWAT was removed from 12-week-old C57BL/6 mice to sex-matched 21-month-old C57BL/6 mice. After euthanasia of donor mice by cervical dislocation, BAT or pgWAT was removed and incubated in 10 ml saline at 37 °C for 20–30 min. Twenty-one-month-old C57BL/6 recipient mice were anesthetized by isoflurane (2–3% in 100% O_2) and BAT or pgWAT from 12-week-old C57BL/6 mice was transplanted into the visceral cavity^{13,50}. The transplant was carefully lodged deep between folds within the endogenous epididymal fat of the recipient. Mice that were sham-operated underwent the same procedure, but

instead of receiving BAT or pgWAT, their epididymal fat pad was located, exposed, and then replaced.

Body composition

Body weight was measured using an OHAUS NV212 scale. The body composition, including fat mass and lean mass, was evaluated by echo-MRI instrument (EchoMRI LLC) with canola oil calibration^{15,49,51}.

Glucose and insulin tolerance test

For glucose tolerance tests, animals were fasted overnight (20:00–8:00) with free access to drinking water. A baseline blood sample was collected from the tail of fully conscious mice, followed by intraperitoneal (i.p.) injection of glucose (2.0 g/kg body weight), and blood was taken from the tail at 15, 30, 60, 90, and 120 min after injection. Insulin tolerance test (ITT) was performed at 12 weeks after transplantation. Animals were fasted for 2 h (12:00–14:00), and baseline blood samples were collected from the tail of fully conscious mice. Insulin (1 U/kg body weight) (Humulin; Eli Lilly) was administered by i.p. injection, and blood samples were taken from the tail at 10, 15, 30, 45, and 60 min after injection. Glucose concentrations were determined from blood using an OneTouch Ultra portable glucometer (LifeScan)^{15,49,51}.

Acute injection of 12,13-diHOME

10 $\mu\text{g/kg}$ body weight of 12,13-diHOME (Cayman Chemical, #10009832) or the structural analog 9,10-diHOME¹⁵ (Cayman Chemical, #53400) as a vehicle was infused into the jugular vein of aged male and female mice. The infusion was administered at a constant rate, with a total volume of 10 mL/kg body weight. Afterward, cardiac PV analysis was performed and blood was immediately removed by cardiac puncture to assess 12,13-diHOME concentration.

TNT-Ephx1/2 treatment

TNT devices were fabricated from double-side polished silicon wafers, as reported previously^{15,42,52,53}. Briefly, projection lithography was used to define 400–500 nm on a photoresist. Deep reactive ion etching was then used drill nanochannels through the exposed Si surface. The backside of the wafers was then patterned with an array of 50- μm openings via standard photolithography followed by deep reactive ion etching to gain fluidic access to the nanochannels. A 50-nm-thick insulating layer of Si_3N_4 was deposited on the wafers via plasma-enhanced chemical vapor deposition (Supplementary Fig. 11)⁴². The Sham mice received TNT with a Sham (empty vector) plasmid to serve as a control group in the experiment¹⁵.

All plasmids (Ephx1 and 2) were purchased from Origene and expanded in *Escherichia coli* following standard procedures⁴². Before TNT, each plasmid was diluted in PBS to a final concentration of 0.05 $\mu\text{g}/\mu\text{L}$ and loaded into the plasmid reservoir of the TNT device. The fur was removed, and the skin was exfoliated. The TNT device was then put in contact with the skin, juxtaposed to an intradermal positive electrode. The negative electrode was inserted into the plasmid reservoir, and a pulsed electric field (250 V, 10-ms pulses, 10 pulses) was applied across electrodes. Approximately 2–3 cm^2 were TNT-treated per mouse. This procedure was conducted directly on the skin that overlies suprascapular and inguinal BAT and white adipose tissue deposits, respectively, beginning in mice who were 21 months of age and was repeated weekly for a total of 6 weeks^{15,42}.

Lipidomic profiling and 12,13-diHOME quantification

We measured circulating 12,13-diHOME by ELISA (Cayman Chemical, #501720) or by LC-MS/MS-based lipidomics calibration curves for 12,13-diHOME were constructed using standard solutions. For all mouse experiments, blood was taken by cardiac puncture. For lipidomics, all lipid standards were purchased from the Cayman Chemical Company. C18SPE cartridges were purchased from Biotage.

All solvents are of high-performance liquid chromatography or liquid chromatography/mass spectrometry (MS) grade and were acquired from Sigma-Aldrich, Fisher Scientific, or VWR International. Aliquots of 100 μ L serum were extracted using methanol and methyl tert-butyl ether (MTBE), followed by water-induced phase separation. The organic phase was collected and cleaned up using C18 SPE cartridges. Samples were dried under nitrogen and reconstituted in 50% methanol⁵. MS analysis was performed on a SCIEX TripleTOF 6600+ system using the high-resolution multiple-reaction monitoring strategy consisting of a time of flight MS experiment looped with multiple MS/MS experiments⁵. Chromatographic separation was performed using a reverse-phase C18 column (2.1 \times 100 mm, 1.7 μ m). Mobile phases consisted of water with 0.1% formic acid (A) and acetonitrile/isopropanol (70:30) with 0.1% formic acid (B), at a flow rate of 0.3 mL/min and a column temperature of 40 °C. The identity of a component was confirmed using PeakView software (SCIEX), and quantification was performed using MultiQuant software (SCIEX). The quantification of 12,13-diHOME was performed against a standard calibration curve built with 15 points ranging from 0.01 pg/ μ L to 1000 pg/ μ L. Internal standards were included for normalization. Obtained values were corrected with the corresponding internal standard. All measurements were performed in a blinded fashion^{12,14,15}.

In vivo cardiac function

Mice were anesthetized with 1–2% isoflurane and echocardiography was performed using a Vevo 3100 Ultrasound. Echocardiogram data were analyzed using VevoLab software^{15,49,54}.

Cardiac pressure–volume analysis

Cardiovascular function was assessed using a 0.33 mm pressure–volume (PV) catheter (Millar, Houston, TX) attached to the MPVS interface (AD Instruments, Colorado Springs, CO). Mice were anesthetized under isoflurane (3–4% in 1–1.5 L/min O₂), intubated, and attached to a ventilator (Harvard Apparatus, Holliston, MA) under constant isoflurane. The cardiac cavity was then surgically exposed and mice were administered intravenous 10% bovine serum albumin (BSA) 90% saline to account for any loss of blood. The left ventricle was pierced apically with a 26 G needle and the catheter was inserted to obtain pressure and volume measurements. Temperature was maintained at a baseline of 37.3 °C throughout the procedure using a temperature-controlling heating pad (Physitemp, Clifton, NJ). All measurements and analyses were performed using LabChart7 (AD Instruments, Colorado Springs, CO)⁵³.

In vivo glucose uptake

In vivo glucose uptake was measured after 12 weeks of BAT transplantation or sham surgery in aged mice. Mice were injected intraperitoneally with 2-DG following an overnight fast. Fluorescence imaging was performed using an IVIS system under isoflurane anesthesia. Fluorescence intensity in regions of interest (ROIs) was quantified using IVIS software⁵⁵.

Measurements of fibrosis

Mouse LV sections were formalin-fixed (10%) and stained with Masson's trichrome. Collagen content was quantified as interstitial area and percent perivascular fibrosis⁵⁶. All histologic analyses were performed by blinded investigators.

Semi-quantitative PCR and quantitative real-time PCR

Tissue processing and quantitative PCR (qPCR) were performed^{51,54,57}. Tissue for qPCR was flash frozen and stored at –80 °C until processing. mRNA was measured by qRT-PCR (Roche LightCycler 480II) using SYBR Green detection (QuantaBio). Sigma-Aldrich custom primers were used for genes of ER stress (ATF4, ATF6, Hspa1b, XBP1, Hspa5, GADD34 and Chop), inflammation (IL-6, IL-1 β , TGF- β , and TNF- α),

oxidative stress (SOD1, SOD2, Nrf2, and Gpx1) and BAT-related (Ephx1, Ephx2, PGC1 α , UCPI, and GLUT4) with the sequences shown in Supplementary Table 9. All qPCR gene expression was normalized to the housekeeping gene RLP7 or β -actin. sXBP1 levels were assessed by semi-qPCR and were calculated as a ratio to usXBP1, with the control group set to one²¹.

Assessment of CaMKII expression and activity

The pCaMKII and total CaMKII expression levels are measured by immunoblotting^{51,58}. The phosphorylated CaMKII at Thr286/287 (pCaMKII) (Thermo Fisher; PA5-37833; 1:1000), and CaMKII (Badrilla; A010-56AP; 1:1000) antibodies were commercially sourced. For the in vitro CaMKII activity model, the 12,13-diHOME incubation (0–25 μ M) was carried out for 5 min in the presence of 32P (2.5 mCi) with ~800 mcg CaMKII δ (Fisher Scientific, PV3978) in a volume of 100 μ L in reaction buffer.

Microscale thermophoresis (MST) assay

We used MST assay to measure the specific binding of 12,13-diHOME (Cayman Chemical, # 10009832), to CaMKII δ protein (ThermoFisher, #PV3978). CaMKII protein is labeled with maleimide 2nd generation dye that is reactive to the thiol groups in cysteine amino acids. Unlabeled 12,13-diHOME was titrated against a fixed concentration of 50 nM labeled CaMKII δ protein that is either preincubated with or without ATP. The measurements were carried out using Monolith 2020 (TNG) instrument (Nanotemper). All the reactions were performed using an assay buffer containing HEPES pH 7.4, 150 mM NaCl, and 0.05% tween-20 in premium capillaries, and the compound was dissolved in a final concentration of 5% DMSO. The data were recorded at room temperature using the nano-red laser at 60% with medium laser power. Data analyses were performed with Prism 9 software, and the data were plotted using the non-linear regression method with the single-site binding model.

Cell culture

For mouse fibroblasts, after anesthesia with isoflurane, mice underwent cervical dislocation. Hearts were extracted and minced in a solution of trypsin (2 mg/mL) dissolved in Hanks Buffered Saline Solution (HBSS) and were incubated overnight. Culture medium stopped trypsin digestion, heart pieces were washed with ice-cold HBSS and collagenase Type II (Worthington Biochem: L5004174) was dissolved in HBSS. Heart pieces were repeatedly shaken then pipetted to dissociate tissue into single cells and supernatant was drawn off and added to a solution of culture medium to inhibit over digestion. Fibroblasts were centrifuged and then resuspended in DMEM growth medium (Gibco: 10313-021) supplemented with 10% FBS (Atlanta Biologicals: S11195H) and 1% each of Anti-Antibiotic-antimycotic (Gibco 15240-062, 100 mL) and L-Glutamine (Sigma: G7513, 20 mL). Cells were grown for 5–7 days to 80–100% confluency at 37 °C in 5% CO₂.

Human cardiac fibroblasts were enzymatically isolated from nonfailing left ventricular tissue and were minced in 2 mg/mL collagenase II (Worthington Biochem: L5004174) dissolved in 1 \times Ham's F-10 buffer (Gibco: 11550043). After digestion, the extract was filtered and centrifuged. The supernatant was discarded, and cells were resuspended in DMEM (Gibco: 10313-021); supplemented with 10% FBS (Atlanta Biologicals: S11195H), 1% L-glutamine (Sigma: G7513), and 1% Antibiotic Antimycotic (Gibco: 15240-062). Cells were allowed to adhere to culture plates for ~4–5 h before removing media containing nonadherent cells (e.g., endothelial, myocytes). Fresh feeding media were replenished, and cells were grown for 5–7 days to 80% to 100% confluency at 37 °C in 5% CO₂⁵⁹. Cardiac fibroblasts were treated 5 μ M AngII (R&D Systems: 1158), 200 nM OA (Sigma-Aldrich: O9381), 1 μ M tunicamycin (Sigma-Aldrich: T7765) for 24 h and 1 μ M 12,13-diHOME for 1 h and those of controls (PBS).

Seahorse bioanalyzer

Isolated fibroblasts (25,000 per well) were seeded onto laminin-coated Seahorse Plates (Agilent) according to standard protocols. Cells were treated for 1 h with 10 μ M 12,13-diHOME or were untreated. The oxygen-consumption rates (OCR; indicating mitochondrial respiration) and extracellular acidification rates (ECAR; indicating glycolysis rate) were monitored in a Seahorse XF24 instrument using the standard protocol of 3-min mix, 2-min wait and 3-min measure. Carbonyl cyanide-p-trifluoromethoxy-phenylhydrazon (FCCP; 2 μ M) was used to determine the cells maximal respiratory capacity by allowing the electron transport chain to function at its maximal rate (maximal respiratory capacity is derived by subtracting non-mitochondrial respiration from the FCCP rate). Oligomycin (a complex V inhibitor; 2 μ M) was used to derive ATP-linked respiration (by subtracting the oligomycin rate from baseline cellular OCR) and proton leak respiration (by subtracting non-mitochondrial respiration from the oligomycin rate). Antimycin A/Rotenone (mitochondrial inhibitors; 0.5 μ M) was used to determine non-mitochondrial respiration. Data from wells of the same treatment group were averaged together and analyzed directly using Waves software. For the normalization of respiration to protein content, cells were lysed in RIPA buffer and protein concentration was measured by Bradford assay.

Bulk RNA-seq analysis

Heart tissues were collected from young, aged, and +BAT-aged male mice. Differentially Expressed Genes (DEGs) were determined using the Benjamin and Hochberg false discovery rate (FDR) correction method to address multiple testing. A volcano plot was generated using GraphPad Prism (version 10) to identify significantly differentially expressed genes. For visualization of expression patterns across samples, a heat map was constructed using hierarchical clustering based on normalized expression values, using MetaboAnalyst (version 6.0) (<https://www.metaboanalyst.ca/MetaboAnalyst/faces/home.xhtml>). GO analysis was conducted to elucidate the cellular components associated with the differentially expressed genes, utilizing Metascape (<https://metascape.org/gp/index.html#/main/step1>) in October 2020.

Statistics

The data are presented as mean \pm SEM or mean \pm SD as indicated in figure legends. Statistical significance was defined as $P < 0.05$. To compare between groups, after assessing the normal distribution, we performed appropriate statistical analyses, including Student's *t* tests for normally distributed data, ANOVA with Tukey's post hoc analysis for parametric data, and the Mann-Whitney U test or Kruskal-Wallis test for nonparametric data. All statistical analyses will be performed using SPSS (ver 20) or GraphPad Prism (version 10).

Reporting summary

Further information on research design is available in the Nature Portfolio Reporting Summary linked to this article.

Data availability

Source data are provided within this paper. The lipidomics data generated in this study have been deposited in the MetaboLights database under accession code (MTBLS12646). The RNA-seq data have been deposited in the NCBI SRA under Accession No. PRJNA1291650. The lipidomics and RNA-seq data generated in this study are also provided in the Supplementary information/Source data file. Additional data that support the findings of this study are available from the corresponding author upon reasonable request. Correspondence and requests for materials should be addressed to K.I.S. Source data are provided with this paper.

References

- Angell, S. Y. et al. The American heart association 2030 impact goal: a presidential advisory from the american heart association. *Circulation* **141**, e120–e138 (2020).
- Chia, C. W., Egan, J. M. & Ferrucci, L. Age-related changes in glucose metabolism, hyperglycemia, and cardiovascular risk. *Circ. Res.* **123**, 886–904 (2018).
- Li, H. et al. Targeting age-related pathways in heart failure. *Circ. Res.* **126**, 533–551 (2020).
- Xie, S., Xu, S.-C., Deng, W. & Tang, Q. Metabolic landscape in cardiac aging: insights into molecular biology and therapeutic implications. *Signal Transduct. Target. Ther.* **8**, 114 (2023).
- Janczewski, A. M. & Lakatta, E. G. Modulation of sarcoplasmic reticulum Ca²⁺ cycling in systolic and diastolic heart failure associated with aging. *Heart Fail. Rev.* **15**, 431–445 (2010).
- Cypess, A. M. et al. Identification and importance of brown adipose tissue in adult humans. *N. Engl. J. Med.* **360**, 1509–1517 (2009).
- Yoneshiro, T. et al. Age-related decrease in cold-activated brown adipose tissue and accumulation of body fat in healthy humans. *Obesity* **19**, 1755–1760 (2011).
- Fuse, S. et al. Brown adipose tissue density measured by near-infrared time-resolved spectroscopy in Japanese, across a wide age range. *J. Biomed. Opt.* **23**, 1 (2018).
- Nirengi, S. & Stanford, K. Brown adipose tissue and aging: a potential role for exercise. *Exp. Gerontol.* **178**, 112218 (2023).
- Becher, T. et al. Brown adipose tissue is associated with cardio-metabolic health. *Nat. Med.* **27**, 58–65 (2021).
- Raiko, J., Orava, J., Savisto, N. & Virtanen, K. A. High brown fat activity correlates with cardiovascular risk factor levels cross-sectionally and subclinical atherosclerosis at 5-year follow-up. *Arterioscler. Thromb. Vasc. Biol.* **40**, 1289–1295 (2020).
- Stanford, K. I. et al. 12,13-diHOME: An exercise-induced lipokine that increases skeletal muscle fatty acid uptake. *Cell Metab.* **27**, 1111–1120.e3 (2018).
- Stanford, K. I. et al. Brown adipose tissue regulates glucose homeostasis and insulin sensitivity. *J. Clin. Investig.* **123**, 215–223 (2013).
- Lynes, M. D. et al. The cold-induced lipokine 12,13-diHOME promotes fatty acid transport into brown adipose tissue. *Nat. Med.* **23**, 631–637 (2017).
- Pinckard, K. M. et al. A novel endocrine role for the BAT-released lipokine 12,13-diHOME to mediate cardiac function. *Circulation* **143**, 145–159 (2021).
- Yuan, J.-J. et al. Quantitative profiling of oxylipins in acute experimental intracerebral hemorrhage. *Front. Neurosci.* **14**, 777 (2020).
- Gabbs, M., Leng, S., Devassy, J. G., Monirujjaman, M., & Aukema, H. M. Advances in our understanding of oxylipins derived from dietary PUFAs. *Adv. Nutr.* **6**, 513–540 (2015).
- Tourdot, B. E., Ahmed, I. & Holinstat, M. The emerging role of oxylipins in thrombosis and diabetes. *Front. Pharm.* **4**, 176 (2014).
- Funk, C. D. Prostaglandins and leukotrienes: advances in eicosanoid biology. *Science* **294**, 1871–1875 (2001).
- Misheva, M. et al. Oxylipin metabolism is controlled by mitochondrial β -oxidation during bacterial inflammation. *Nat. Commun.* **13**, 139 (2022).
- Yoon, S.-B. et al. Real-time PCR quantification of spliced X-box binding protein 1 (XBP1) using a universal primer method. *PLOS One* **14**, e0219978 (2019).
- Prévilon, M., Pezet, M., Vinet, L., Mercadier, J.-J. & Rouet-Benzineb, P. Gender-specific potential inhibitory role of Ca²⁺/calmodulin dependent protein kinase phosphatase (CaMKP) in pressure-overloaded mouse heart. *PLOS One* **9**, e90822 (2014).
- Vidal, R. et al. Transcriptional heterogeneity of fibroblasts is a hallmark of the aging heart. *JCI Insight* **4**, e131092 (2019).

24. Ge, C.-X. et al. Endoplasmic reticulum stress-induced iRhom2 up-regulation promotes macrophage-regulated cardiac inflammation and lipid deposition in high fat diet (HFD)-challenged mice: intervention of fisetin and metformin. *Free Radic. Biol. Med.* **141**, 67–83 (2019).
25. Mekahli, D., Bultynck, G., Parys, J. B., De Smedt, H. & Missiaen, L. Endoplasmic-reticulum calcium depletion and disease. *Cold Spring Harb. Perspect. Biol.* **3**, a004317 (2011).
26. Groenendyk, J., Agellon, L. B., & Michalak, M. Calcium signaling and endoplasmic reticulum stress. *Int. Rev. Cell. Mol. Biol.* 1–20. <https://doi.org/10.1016/bs.ircmb.2021.03.003> (2021).
27. McCluskey, C., Mooney, L., Paul, A. & Currie, S. Compromised cardiovascular function in aged rats corresponds with increased expression and activity of calcium/calmodulin dependent protein kinase II δ in aortic endothelium. *Vasc. Pharm.* **118–119**, 106560 (2019).
28. Santalla, M. et al. Aging and CaMKII alter intracellular Ca²⁺ transients and heart rhythm in *Drosophila melanogaster*. *PLOS One* **9**, e101871 (2014).
29. Kong, L. et al. $\text{scp} > \text{CaMKII} < \text{scp}$ orchestrates endoplasmic reticulum stress and apoptosis in doxorubicin-induced cardiotoxicity by regulating the $\text{scp} > \text{IRE1}\alpha < \text{scp}$ / $\text{scp} > \text{XBP1s} < \text{scp}$ pathway. *J. Cell Mol. Med.* **26**, 5303–5314 (2022).
30. Timmins, J. M. et al. Calcium/calmodulin-dependent protein kinase II links ER stress with Fas and mitochondrial apoptosis pathways. *J. Clin. Investig.* **119**, 2925–2941 (2009).
31. Chi, M. et al. Phosphorylation of calcium/calmodulin-stimulated protein kinase II at T286 enhances invasion and migration of human breast cancer cells. *Sci. Rep.* **6**, 33132 (2016).
32. Erickson, J. R. et al. A dynamic pathway for calcium-independent activation of CaMKII by methionine oxidation. *Cell* **133**, 462–474 (2008).
33. Strait, J. B. & Lakatta, E. G. Aging-associated cardiovascular changes and their relationship to heart failure. *Heart Fail. Clin.* **8**, 143–164 (2012).
34. Pacher, P. et al. Left ventricular pressure-volume relationship in a rat model of advanced aging-associated heart failure. *Am. J. Physiol.-Heart Circ. Physiol.* **287**, H2132–H2137 (2004).
35. Triposkiadis, F., Xanthopoulos, A., Parissis, J., Butler, J. & Farmakis, D. Pathogenesis of chronic heart failure: cardiovascular aging, risk factors, comorbidities, and disease modifiers. *Heart Fail. Rev.* **27**, 337–344 (2022).
36. Halter, J. B. et al. Diabetes and cardiovascular disease in older adults: current status and future directions. *Diabetes* **63**, 2578–2589 (2014).
37. Pinckard, K. M. & Stanford, K. I. The heartwarming effect of brown adipose tissue. *Mol. Pharm.* **102**, 39–50 (2022).
38. Yang, F. T. & Stanford, K. I. Batokines: mediators of inter-tissue communication (a Mini-Review). *Curr. Obes. Rep.* **11**, 1–9 (2022).
39. Ruan, C.-C. et al. A2A receptor activation attenuates hypertensive cardiac remodeling via promoting brown adipose tissue-derived FGF21. *Cell Metab.* **28**, 476–489.e5 (2018).
40. Zhao, H. et al. Small extracellular vesicles from brown adipose tissue mediate exercise cardioprotection. *Circ. Res.* **130**, 1490–1506 (2022).
41. Hernández-Saavedra, D. & Stanford, K. I. The regulation of lipokines by environmental factors. *Nutrients* **11**, 2422 (2019).
42. Gallego-Perez, D. et al. Topical tissue nano-transfection mediates non-viral stroma reprogramming and rescue. *Nat. Nanotechnol.* **12**, 974–979 (2017).
43. Mariángelo, J. I. E., Valverde, C. A., Vittone, L., Said, M. & Mundiña-Weilenmann, C. Pharmacological inhibition of translocon is sufficient to alleviate endoplasmic reticulum stress and improve Ca²⁺ handling and contractile recovery of stunned myocardium. *Eur. J. Pharm.* **914**, 174665 (2022).
44. Du, L. et al. eNOS/iNOS and endoplasmic reticulum stress-induced apoptosis in the placentas of patients with preeclampsia. *J. Hum. Hypertens.* **31**, 49–55 (2017).
45. Wang, S. et al. Endoplasmic reticulum stress in the heart: insights into mechanisms and drug targets. *Br. J. Pharm.* **175**, 1293–1304 (2018).
46. Preetha Rani, M. R. et al. In vitro and in vivo studies reveal the beneficial effects of chlorogenic acid against ER stress mediated ER-phagy and associated apoptosis in the heart of diabetic rat. *Chem. Biol. Interact.* **351**, 109755 (2022).
47. Maamoun, H., Benameur, T., Pintus, G., Munusamy, S., & Agouni, A. Crosstalk between oxidative stress and endoplasmic reticulum (ER) stress in endothelial dysfunction and aberrant angiogenesis associated with diabetes: a focus on the protective roles of heme oxygenase (HO)-1. *Front. Physiol.* **10**, 70 (2019).
48. HOSHINO, K. Transplantability of mammary gland in brown fat pads of mice. *Nature* **213**, 194–195 (1967).
49. Peres Valgas da Silva, C. et al. Brown adipose tissue prevents glucose intolerance and cardiac remodeling in high-fat-fed mice after a mild myocardial infarction. *Int. J. Obes.* **46**, 350–358 (2022).
50. Tran, T. T., Yamamoto, Y., Gesta, S. & Kahn, C. R. Beneficial effects of subcutaneous fat transplantation on metabolism. *Cell Metab.* **7**, 410–420 (2008).
51. Dewal, R. S. et al. Phospho-ablation of cardiac sodium channel Nav1.5 mitigates susceptibility to atrial fibrillation and improves glucose homeostasis under conditions of diet-induced obesity. *Int. J. Obes.* **45**, 795–807 (2021).
52. Diaz-Starokozheva, L. et al. Early Intervention in ischemic tissue with oxygen nanocarriers enables successful implementation of restorative cell therapies. *Cell Mol. Bioeng.* **13**, 435–446 (2020).
53. Tanwar, V. et al. In utero particulate matter exposure produces heart failure, electrical remodeling, and epigenetic changes at adulthood. *J. Am. Heart Assoc.* **6**, e005796 (2017).
54. Peres Valgas Da Silva, C. et al. Exercise training after myocardial infarction increases survival but does not prevent adverse left ventricle remodeling and dysfunction in high-fat diet fed mice. *Life Sci.* **311**, 121181 (2022).
55. BonDurant, L. D. et al. FGF21 regulates metabolism through adipose-dependent and -independent mechanisms. *Cell Metab.* **25**, 935–944.e4 (2017).
56. DuPont, J. J., Kim, S. K., Kenney, R. M. & Jaffe, I. Z. Sex differences in the time course and mechanisms of vascular and cardiac aging in mice: role of the smooth muscle cell mineralocorticoid receptor. *Am. J. Physiol. Heart Circ. Physiol.* **320**, H169–H180 (2021).
57. Lessard, S. J. et al. Resistance to aerobic exercise training causes metabolic dysfunction and reveals novel exercise-regulated signaling networks. *Diabetes* **62**, 2717–2727 (2013).
58. Nassal, D. M. et al. Ca²⁺/calmodulin kinase II-dependent regulation of β IV-spectrin modulates cardiac fibroblast gene expression, proliferation, and contractility. *J. Biol. Chem.* **297**, 100893 (2021).
59. Patel, N. J. et al. β IV-spectrin/STAT3 complex regulates fibroblast phenotype, fibrosis, and cardiac function. *JCI Insight* **4**, e131046 (2019).

Acknowledgements

This work was supported by NIH grants R01AG060542 to K.I.S. and P.M.C., R01DK133859-01A1 to K.I.S. and D.G.P., R01HL171689, R01HL165751 and R01HL156652 to T.J.H., K01AG044437 to P.M.C., R01DK1122835, R01DK099511, and P30DK036836 to L.J.G. and Joslin Diabetes Center, and DP1DK126199 and DP2 EBO28110 to D.G.P. K.M.P. was supported by F31-HL152648-01A1 and T32-HL134616, B.B. was supported by T32HL149637. S.N. was supported by a Grant-in-Aid for Scientific Research from the Ministry of Education, Culture, Sports, Science, and Technology of Japan (17J11622 and 20K19532), Kao Research Council for the Study of Healthcare Science, and American

Heart Association Career Development Award (25CDA1444322). P.V. was supported by AHAPRE903654. E.F.S. was supported by AHA POST906327. BioRender provided the platform used to create the schematic illustration (Agreement number: SB28FMSC8L).

Author contributions

This study was conceived and designed by S.N. and K.I.S. P.M.C., L.J.G., and R.J.W.M. were responsible for the human samples. Human lipidomics data were analyzed by P.M.C., S.N., and K.I.S. Mouse in vivo experiments were carried out by S.N., C.P.V.S., L.A.B., P.V., R.S.D., K.M.P., T.S., H.H., and M.G. and supervised by K.I.S. and L.E.W. RNA-seq data were analyzed by S.N., C.P.V.S., and D.H.S. Lipidomics experiments were performed by V.B., J.H., and M.A.K. TNT experiments were performed by S.N., D.D., K.D., and S.D.S. and supervised by D.G.P. In vitro experiments were performed by S.N., B.B., J.C., A.G., and L.A.B. and supervised by A.L.M., T.J.H., and K.I.S. H.S.H. and K.C. performed and analyzed the biophysical characterization data. S.N. and K.I.S. analyzed and interpreted the data, prepared figures, and completed statistical analysis. The manuscript was written by S.N. and K.I.S. with input from other authors. K.I.S. is the guarantor of this work and, as such, had full access to all the data in the study and takes responsibility for the integrity of the data and the accuracy of the data analysis. All authors gave final approval for publication.

Competing interests

K.I.S. and D.G.P. are co-inventors of US Patent # 20230279372, which is related to tissue nano transfection technology. The other authors have no competing interests.

Additional information

Supplementary information The online version contains supplementary material available at <https://doi.org/10.1038/s41467-025-62474-7>.

Correspondence and requests for materials should be addressed to Kristin I. Stanford.

Peer review information *Nature Communications* thanks the anonymous reviewers for their contribution to the peer review of this work. A peer review file is available.

Reprints and permissions information is available at <http://www.nature.com/reprints>

Publisher's note Springer Nature remains neutral with regard to jurisdictional claims in published maps and institutional affiliations.

Open Access This article is licensed under a Creative Commons Attribution-NonCommercial-NoDerivatives 4.0 International License, which permits any non-commercial use, sharing, distribution and reproduction in any medium or format, as long as you give appropriate credit to the original author(s) and the source, provide a link to the Creative Commons licence, and indicate if you modified the licensed material. You do not have permission under this licence to share adapted material derived from this article or parts of it. The images or other third party material in this article are included in the article's Creative Commons licence, unless indicated otherwise in a credit line to the material. If material is not included in the article's Creative Commons licence and your intended use is not permitted by statutory regulation or exceeds the permitted use, you will need to obtain permission directly from the copyright holder. To view a copy of this licence, visit <http://creativecommons.org/licenses/by-nc-nd/4.0/>.

© The Author(s) 2025

¹Dorothy M. Davis Heart and Lung Research Institute, The Ohio State University Wexner Medical Center, Columbus, OH, USA. ²Department of Surgery, Division of General and Gastrointestinal Surgery, The Ohio State University Wexner Medical Center, Columbus, OH, USA. ³Department of Physiology and Cell Biology, The Ohio State University Wexner Medical Center, Columbus, OH, USA. ⁴Division of Preventive Medicine, Clinical Research Institute, National Hospital Organization Kyoto Medical Center, Kyoto, Japan. ⁵Department of Internal Medicine, Division of Cardiovascular Medicine, The Ohio State University, Columbus, OH, USA. ⁶Department of Biomedical Engineering, The Ohio State University, Columbus, OH, USA. ⁷Department of Internal Medicine, Division of Pulmonary, Critical Care and Sleep Medicine, The Ohio State University, Columbus, OH, USA. ⁸Department of Surgery, Division of Cardiac Surgery, The Ohio State University Wexner Medical Center, Columbus, OH, USA. ⁹BGPBio, Framingham, MA, USA. ¹⁰Section on Integrative Physiology and Metabolism, Joslin Diabetes Center, Harvard Medical School, Boston, MA, USA. ¹¹Translational Research Institute for Metabolism and Diabetes, AdventHealth, Orlando, FL, USA. ✉ e-mail: Kristin.Stanford@osumc.edu